Available online at www.sciencedirect.com
ScienceDirect
Trans. Nonferrous Met. Soc. China 35(2025) 1000−1016
Transactions of Nonferrous Metals Society of China
www.tnmsc.cn

Kinetic study of ultrasonic-assisted vanadium(V) adsorption by supported bifunctionalizedized ionic liquid

Jia-hao ZHOU[1,2], Shen-xu BAO[1,2,3], Yi-min ZHANG[1,2,3,4],
Bo CHEN[1,2], Yu LIANG[1,2], Xiao-chuan HOU[5], Si-yuan YANG[1,2], Yang PING[6]

1. Key Laboratory of Green Utilization of Critical Non-metallic Mineral Resources, Ministry of Education, Wuhan University of Technology, Wuhan 430070, China;
2. School of Resources and Environmental Engineering, Wuhan University of Technology, Wuhan 430070, China;
3. Hubei Key Laboratory of Mineral Resources Processing and Environment, Wuhan 430070, China;
4. State Environmental Protection Key Laboratory of Mineral Metallurgical Resources Utilization and Pollution Control, Wuhan University of Science and Technology, Wuhan 430081, China;
5. Zhejiang New Era Zhongneng Recycling Technology Co., Ltd., Shaoxing 312000, China;
6. Powerchina Eco-environmental Group Co., Ltd., Shenzhen 518102, China

Received 21 July 2023; accepted 17 April 2024

Abstract: The adsorption kinetics of polystyrene [1-butyl-3-methylimidazolium][bis(2,4,4-trimethylpentyl)phosphinate] (PS[C_4mim][C272]) towards V(V) in acidic leachate was explored under ultrasound. The effects of ultrasonic power and V(V) concentration on the adsorption performance of PS[C_4mim][C272] were investigated. The results showed that ultrasonic radiation significantly shortened the adsorption equilibrium time and improved the adsorption performance of PS[C_4mim][C272] compared with the conventional oscillation. At an ultrasonic power of 200 W, the equilibrium adsorption capacity of PS[C_4mim][C272] reached its maximum of 311.58 mg/g. The kinetic model fitting results showed that the adsorption process of PS[C_4mim][C272] strictly followed the pseudo-second-order kinetic model under ultrasound. Analysis using the shrinking core model and the Weber−Morris model showed that the adsorption process of PS[C_4mim][C272] was primarily controlled by intra-particle diffusion mechanism. The adsorption isotherm model study showed that the Langmuir isotherm model could effectively fit the adsorption process of PS[C_4mim][C272] under ultrasound.

Key words: kinetics; ultrasound; vanadium; polystyrene [1-butyl-3-methylimidazolium][bis(2,4,4-trimethylpentyl)-phosphinate]; conventional oscillation; adsorption

1 Introduction

Vanadium, a rare high-melting-point metal with excellent physical, chemical, and catalytic properties, is one of the strategic metals of the country [1]. Vanadium and its compounds are widely used in industrial fields, such as steel, non-ferrous alloys, chemical industry, refining, glass, and ceramics [2]. Most vanadium is extracted by acid leaching from vanadium-bearing resources and the vanadium concentration in acidic leachate is low [3]. Extraction and ion exchange are commonly used to enrich metal ions in leachate, but they have drawbacks such as complex operation, low processing capacity, and large reagent usage. Therefore, new adsorption materials need to be developed. Ionic liquids (ILs) are a new type of “designable” green

Corresponding author: Shen-xu BAO, Tel: +86-13387592291, E-mail: sxbao@whut.edu.cn
DOI: https://doi.org/10.1016/S1003-6326(24)66730-0

solvents, and immobilizing them on carriers is an effective way to solve the above problems. By modifying the cations and anions of ILs with different functional groups, bifunctionalized ionic liquids with different physical and chemical properties can be obtained [4]. As a new type of functional composite material adsorbent in recent years, supported bifunctionalized ionic liquids (SBILs) have attracted widespread attention in the enrichment of metals due to their excellent extraction performance and selectivity [4,5]. The large specific surface area, porous structure and abundant functional groups of SBILs can provide sufficient adsorption sites for vanadium, and thus they have been proved to be good materials for metal adsorption [6]. This study investigated the adsorption characteristics and kinetics of PS[C_4mim][C272] prepared for V(V).

Currently, the enrichment process of vanadium from leaching solutions is usually carried out in a constant temperature water bath oscillator [6,7], or magnetic stirrer [8]. However, these conventional reaction processes have problems such as long adsorption equilibrium time and decreased stability of cycling adsorption. This leads to low product lifespan and high raw material consumption, which seriously hinders industrial applications. Therefore, it is of great significance to develop effective methods to improve the adsorption performance of vanadium on supported ILs.

As one of the forefront fields in chemical research [9,10], sonochemistry has wide adaptability to various systems, and its application fields are continuously expanding [11,12], especially in chemical reaction intensification, chemical process intensification, wastewater treatment, and new material synthesis [13,14]. The application of ultrasound in mass transfer separation is also very active, and many studies have been reported on the adsorption and desorption processes of porous materials (e.g., resins, activated carbon, and rubber) under ultrasound [15−17]. Many applications of ultrasound are mainly based on the cavitation effect generated by ultrasound, which refers to the appearance of tiny bubbles in a liquid under a certain ultrasonic intensity [13,18]. These extreme conditions create high temperature, high pressure, and high-speed microjets when the cavitation bubbles bursts can significantly enhance mass transfer processes, increase reaction rates, and may simultaneously improve the interaction between the solute and the adsorbent [19−21]. The primary resistance to mass transfer in porous materials is the concentration diffusion of solutes between the solution and the adsorption surface. Therefore, utilizing the cavitation effect generated by ultrasound can reduce the thickness of the mass transfer boundary layer and increase the creep in pores to improve the total mass transfer efficiency and rate.

Ultrasound has unparalleled advantages over traditional mechanical methods, such as stirring and vibration in the above aspects. Based on current research [16], it can be found that ultrasonic field not only enhances the mass transfer in the adsorption process of polymer resin and activated carbon, but also improves the reaction rate constant and particle diffusion coefficient [22]. ENTEZARI et al [23] studied the effect of ultrasound on Cd(II) adsorption in waste tire rubber. The results showed that the cavitation effect of ultrasound strengthened the diffusion of solute inside the rubber. Under ultrasound conditions, the diffusion coefficient of tire rubber was about three times that under normal conditions. WEN et al [24] studied the adsorption performance and mechanism of ion exchange resin (201×8) on uranium in leach solution under ultrasonic. The results showed that the introduction of ultrasound could increase the adsorption capacity of the resin by more than 15%. The adsorption capacity, reaction rate constant and particle diffusion coefficient of the resin increased with the increase of ultrasonic power. The particle diffusion coefficient under ultrasound was about twice that in the absence of ultrasound.

Ultrasound-assisted recovery of metals from leach solutions offers an exciting opportunity for efficient resource utilization. In addition, the application of SBILs as adsorbents for vanadium extraction process becomes a sustainable and green approach [25]. The application of ultrasound-assisted SBILs for vanadium adsorption and the optimization of adsorption kinetics are less studied, and more comprehensive studies are needed to understand the effect of ultrasound on vanadium adsorption processes and mechanisms. Therefore, in order to solve the issues of long adsorption

equilibrium time and low adsorption performance in existing processes, this study proposed a method to optimize the adsorption process by introducing ultrasound. By comparing experimental results under ultrasound-assisted and conventional oscillation adsorption conditions, the potential of ultrasound in enhancing the adsorption rate and performance of PS[C_4mim][C272] for V(V) was evaluated. The kinetics and isotherm models of vanadium adsorption onto PS[C_4mim][C272] were discussed in detail, revealing the mechanism of ultrasound's influence on the adsorption process. Different characterization techniques were employed to analyze the changes in functional groups and microstructure of PS[C_4mim][C272] before and after adsorption. Additionally, the recycling feasibility of PS[C_4mim][C272] under ultrasonic-assisted and conventional oscillation conditions were compared. This study will provide a novel idea to improve the adsorption performance of the adsorbent towards other metals in complex aqueous solutions with the assistance of ultrasound.

2 Experimental

2.1 Raw materials and reagents

The preparation of PS[C_4mim][C272] was carried out according to our previous studies [6]. Supported 1-butyl-3-methylimidazole chloride ILs (PS[C_4mim][Cl]) were subjected to anion exchange with bis(2,4,4-trimethylpentyl) phosphine acid (Cyanex272) to prepare PS[C_4mim][C272] under certain conditions. The vanadium(V)-containing leaching solution was prepared by dissolving sodium metavanadate in ultrapure water [26,27], and the pH of the vanadium(V)-containing solution was adjusted using concentrated sulfuric acid. Both sodium metavanadate and concentrated sulfuric acid are analytical grades provided by Shanghai McLean Biochemical Technology Co., Ltd. Other reagents used in this experiment are also of analytical grade.

2.2 Instruments and characterization methods

Routine oscillation adsorption experiments were carried out in a constant temperature water bath oscillator (SHA-2 type, Jiangsu Jintan Yitong Electronics Co., Ltd.). Ultrasonic adsorption experiments were conducted using an ultrasonic generator (VS-SHX−1500W, Wuxi Wuxin Instrument Manufacturing Co., Ltd.) and a digital intelligent temperature-controlled magnetic stirrer (SZCL−2, Shanghai Borna Instrument Co., Ltd.). The solution pH was measured using a SevenCompact™ pH/ion meter (S220, Mettler-Toledo Instrument Co., Ltd.).

The vanadium content of the solution was determined by the ammonium ferrous sulfate titration method (GB/T 8704.5 — 2020). The functional group types of PS[C_4mim][C272] before and after adsorption were analyzed by FTIR (Nicolet™ iS™ 10, Thermo Nicolet Corporation Co., Ltd.). The overall morphology and structure of PS[C_4mim][C272] were observed by SEM (JSM-IT300, JEOL).

2.3 Adsorption study

The adsorption process of PS[C_4mim][C272] for V(V) under ultrasound was conducted as follows. First, the pH of vanadium(V)-containing solutions with different concentrations was adjusted to the desired value (pH=1.6) [6]. Dry PS[C_4mim][C272] was mixed with the solution by stirring at a liquid−solid (L/S) ratio of 200:1 mL/g. The purpose of mechanical stirring is to disperse PS[C_4mim][C272] evenly in the solution and eliminate the turbulent effect caused by ultrasonic waves. Subsequently, the reaction was conducted at a constant temperature under different ultrasonic powers. The experimental setup is illustrated in Fig. 1. Conventional oscillation process is similar to the ultrasonic-assisted experiment. The difference is that the latter is performed by oscillating at a specific rate for different time in a constant temperature water bath oscillator to complete the reaction.

After certain reaction time, samples were taken from the reaction solution to analyze the concentration of vanadium(V). The capacity of V(V) adsorbed onto PS[C_4mim][C272] was calculated by

$$Q_t=\frac{(C_0-C_t)V}{m} \tag{1}$$

where Q_t is the adsorption capacity of V(V) by PS[C_4mim][C272] at t min (mg/g); C_0 and C_t are the vanadium concentration of the initial and after t min reaction in the solution (mg/L), respectively; V is the volume of the solution (L); m is the mass of PS[C_4mim][C272] (g).

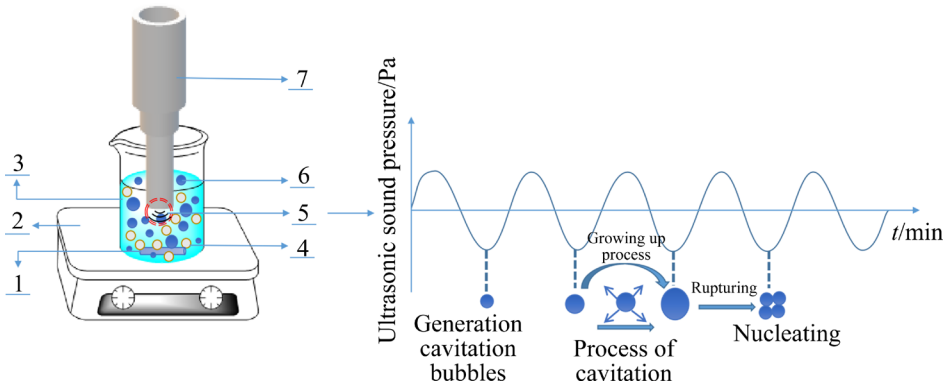

Fig. 1 Schematic diagram of ultrasonic-assisted adsorption: 1−Magnetic rotor; 2−Magnetic agitator; 3−Solution; 4−SBILs; 5−Phenomenon of cavitation; 6−Cavitation bubble; 7−Ultrasonic probe

The reuse potential of PS[C_4mim][C272] was evaluated by examining the effect of ultrasound on the recycling process. Ten adsorption−desorption cycle experiments were performed under ultrasound conditions. After adsorption, the PS[C_4mim][C272] was mixed with a 4 mol/L $NH_3{\cdot}H_2O$ solution at an L/S of 200:1 mL/g in a conical bottle. And the desorption process was completed by oscillating for 7 h in a constant temperature water bath oscillator. The desorption rate (D_V) and the ratio of the adsorption capacity to the initial adsorption capacity (η_n, %) during the nth cycle were calculated by Eqs. (2) and (3), respectively.

$$D_V = \frac{m_{ve}}{m_{v0}} \times 100\% \tag{2}$$

$$\eta_n = \frac{Q_n}{Q} \times 100\% \tag{3}$$

where m_{ve} is the V(V) mass adsorbed by PS[C_4mim][C272] (mg), and m_{v0} is the V(V) mass in the solution after desorption (mg); Q_n is the adsorption capacity of V(V) by PS[C_4mim][C272] in the nth cycle (mg/g), and Q is the initial adsorption capacity of V(V) by PS[C_4mim][C272] (mg/g).

2.4 Study on adsorption model

2.4.1 Adsorption kinetic model

The pseudo-first-order kinetic model based on solid adsorption is the most used equation for the kinetic study of liquid-phase adsorption. The pseudo-second-order kinetic model assumes that the adsorption rate is controlled by the chemical adsorption mechanism, which involves electron sharing or transfer between the adsorbent and the adsorbate. The pseudo-first-order kinetic model [28] and pseudo-second-order kinetic model [29] were used to fit the adsorption process of PS[C_4mim][C272] for V(V) under ultrasound conditions, and the adsorption mechanism was explored. The equations were expressed as Eqs. (4) and (5), respectively.

$$Q_t = Q_e(1 - e^{-k_1 t}) \tag{4}$$

$$Q_t = \frac{k_2 Q_e^2 t}{1 + k_2 Q_e t} \tag{5}$$

where Q_e is the adsorption capacity at the reaction equilibrium (mg/g); k_1 is the pseudo-first-order kinetic equation adsorption rate constant (min^{-1}); k_2 is the pseudo-second-order kinetic equation adsorption rate constant (g/(mg·min)); t is the adsorption time (min).

2.4.2 Shrinking core model

Generally, kinetic models do not provide detailed information about the adsorption mechanism and actual rate-limiting steps during the adsorption process. Different models can analyze this to describe the rate-limiting mechanism of the adsorption process, such as Weber−Morris intra-particle diffusion model [30], Boyd kinetic model [31], and shrinking core model (SCM) [32]. The SCM is currently widely used to describe the adsorption behavior of porous materials [33]. This method is suitable for resins with minor porosity and virtually unaffected by fluid reactants. For solid−liquid adsorption processes, the transfer of adsorbate is usually manifested as liquid film diffusion, intra-particle diffusion, or both. The

ion-pairing reaction of vanadium oxyanions on PS[C_4mim][C272] is similar to other multi-reactions between solid and liquid [34]. A series of rate-controlling steps can describe it: metal ions diffused from the solution through a liquid film to the surface of PS[C_4mim][C272]; metal ions diffused from the surface of PS[C_4mim][C272] to the interior; chemical reactions occurred in metal ions at the active positions inside the PS[C_4mim][C272]. There is usually one step of the three steps with greater resistance to the ion bond reactions than the other two steps, so the slowest step is considered to be the rate-controlling step of the adsorption process [35].

The control equations of liquid film diffusion (Eq. (6)), intra-particle diffusion (Eq. (7)), and chemical reaction (Eq. (8)) in the SCM are respectively expressed as follows:

$$F=\frac{3K_{\mathrm{f}}C_0}{\alpha C_{\mathrm{so}}r}\cdot t \tag{6}$$

$$3-3(1-F)^{2/3}-2F=\frac{6\bar{D}C_0}{\alpha C_{\mathrm{so}}r^2}\cdot t \tag{7}$$

$$1-(1-F)^{1/3}=\frac{K_{\mathrm{c}}C_0}{r}\cdot t \tag{8}$$

where α is the stoichiometric coefficient; F is the adsorption rate (%); K_{f}, $\bar{D}$ and K_{c} are expressed as the liquid film diffusion coefficient (m/s), intra-particle diffusion coefficient (m^2/s), and chemical reaction rate constant (m/s); respectively; C_{so} is the molar concentration of the fixed ionic groups in the unreacted particles (mol/g); r is the particle radius of PS[C_4mim][C272] (m).

The adsorption rate can be calculated by

$$F=\frac{Q_t}{Q_{\mathrm{e}}} \tag{9}$$

When the internal diffusion is the rate-controlling step of the adsorption process, the Weber−Morris intra-particle diffusion model can be used for verification. The calculation equation can be expressed as

$$Q_t=k_{\mathrm{id}}\cdot t^{1/2} \tag{10}$$

where k_{id} is the internal diffusion rate constant (mg/(g·$\mathrm{min}^{1/2}$)).

2.4.3 Diffusion coefficient calculation

If intra-particle diffusion is the rate-controlling step of the adsorption process, the Double-driving force model [36] can be used to calculate the diffusion coefficient, as shown in Eq. (11).

$$\ln(1-F)^2=-\frac{D\pi^2}{r_1^2}\cdot t \tag{11}$$

where D represents the average particle diffusion coefficient of the adsorbent (m^2/s); r_1 represents the average particle radius of the adsorbent (m).

2.4.4 Adsorption isotherm model

The adsorption performance of PS[C_4mim][C272] for V(V) was investigated under the ultrasonic power of 200 W. The Langmuir isotherm model and Freundlich isotherm model [37] were used to fit the adsorption isotherms, expressed as Eqs. (12) and (13), respectively. For the adsorption process consistent with the Langmuir isotherm model, Eq. (14) can be used to calculate the separation factor (R_{L}), so as to evaluate the difficulty of the adsorption process.

$$Q_{\mathrm{e}}=\frac{Q_0K_{\mathrm{L}}C_{\mathrm{e}}}{K_{\mathrm{L}}C_{\mathrm{e}}+1} \tag{12}$$

$$Q_{\mathrm{e}}=K_{\mathrm{F}}C_{\mathrm{e}}^{1/n} \tag{13}$$

$$R_{\mathrm{L}}=\frac{1}{Q_0K_{\mathrm{L}}+1} \tag{14}$$

where C_{e} is the equilibrium concentration (mg/L); K_{L} and K_{F} are the constants of the Langmuir isothermal model (L/mg) and the Freundlich isothermal model ((mg/g)(L/mg)$^{1/n}$), respectively; Q_0 is the theoretical saturated adsorption capacity (mg/g); $1/n$ is an empirical constant, indicating the adsorption strength.

3 Results and discussion

3.1 Effect of ultrasonic power on adsorption process

Adsorption experiments were conducted under different power levels (0, 100, 200, 300, and 400 W) to investigate the changes in the adsorption performance of PS[C_4mim][C272] under ultrasonic-assisted and conventional oscillation. The experimental results are shown in Fig. 2. In Fig. 2, the adsorption rates of PS[C_4mim][C272] are fast under different power conditions, indicating that it is an effective vanadium adsorbent. Within the studied ultrasonic power range, the equilibrium adsorption capacity of PS[C_4mim][C272] for V(V) reaches its maximum value at an ultrasonic power

of 200 W. This is because as ultrasonic power increases from 100 to 200 W, the cavitation effect of ultrasound can generate high-speed microjets, stronger high-pressure shock waves and acoustic eddy currents. These effects continuously impact the pores of PS[C_4mim][C272], and strengthen the mass transfer of vanadium at the boundary layer and deep in the pores, improving the adsorption performance of PS[C_4mim][C272] [38]. However, with further increase in ultrasonic power (300 and 400 W), strong high-pressure shock waves and acoustic eddy currents are generated, causing some bonds to break between IL and the pore surface of PS[C_4mim][C272], as well as between vanadium and the pore surface of PS[C_4mim][C272] [39]. This results in the desorption of vanadium loaded on the surface and the corresponding decrease in equilibrium adsorption capacity. Therefore, at an appropriate ultrasonic power, ultrasonic irradiation can improve the adsorption performance.

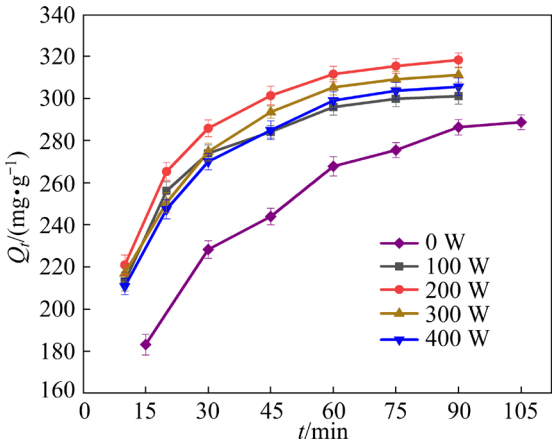

Fig. 2 Effects of ultrasonic power on adsorption properties of PS[C_4mim][C272]

By comparing the equilibrium adsorption capacity of PS[C_4mim][C272] for V(V) under ultrasonic power of 200 W and conventional oscillation, the adsorption curve results show that the adsorption capacity of PS[C_4mim][C272] for V(V) gradually increases with increasing reaction time. Moreover, the adsorption rate and adsorption capacity under ultrasound are higher than those under the conventional oscillation. Under the ultrasound environment, PS[C_4mim][C272] reaches an equilibrium state at 60 min with an equilibrium adsorption capacity of 311.58 mg/g. On the other hand, it takes 90 min for PS[C_4mim][C272] to reach equilibrium under conventional oscillation, and the adsorption capacity is also lower, at 285.49 mg/g. Therefore, at an ultrasonic power of 200 W, ultrasound radiation can significantly enhance the adsorption performance of PS[C_4mim][C272] for V(V).

3.2 Influence of solution concentration on adsorption process

Based on the conclusions in Section 3.1, the effects of different vanadium concentrations on the adsorption performance of PS[C_4mim][C272] under ultrasonic power (200 W) and conventional oscillation conditions were investigated. Four pure solutions with vanadium concentration of 2000, 2500, 3000 and 3500 mg/L were prepared, with the same content of other ions and pH values. The experimental results are shown in Fig. 3. Under both ultrasound and conventional oscillation, the adsorption capacity of PS[C_4mim][C272] for V(V) increases significantly with the increase of vanadium concentration. This is mainly because there are a large number of active adsorption sites on PS[C_4mim][C272] during the initial stage of the reaction. The concentration gradient of the solution increases gradually with the increase of vanadium concentration, resulting in a concentration difference between PS[C_4mim][C272] and the solution. Under the concentration gradient, vanadium oxyanions easily diffuse into the gel network structure of PS[C_4mim][C272]. The probability of PS[C_4mim][C272] binding with V═O or V—O increases [40], and the adsorption capacity of PS[C_4mim][C272] for V(V) increases with the increase of initial vanadium concentration. As the adsorption time continues to increase, the adsorption capacity of PS[C_4mim][C272] gradually approaches saturation and shows no significant change. This is because the vanadium oxyanions gradually occupy the adsorption sites inside PS[C_4mim][C272], and the concentration of vanadium in the solution gradually decreases.

3.3 Adsorption kinetics analysis

The influence of adsorption time on the adsorption capacity of PS[C_4mim][C272] under different ultrasonic power conditions (0, 100, 200, 300 and 400 W) was studied. According to the corresponding goodness of fit (R^2) and consistency between the experimental adsorption capacities and

equilibrium adsorption capacities, the suitability of the experimental data was fitted by nonlinear regression of the pseudo-first-order and pseudo-second-order adsorption kinetic models. The kinetic fitting curve results are shown in Fig. 4, and the essential kinetic parameters obtained from the experimental data fitting are shown in Table 1. From the perspective of R^2 values, the R^2 of the pseudo-second-order kinetic model is higher than the pseudo-first-order model, which is close to 1. Moreover, the Q_e values calculated by the pseudo-second-order kinetic model are in better agreement with the experimental data for different ultrasonic power conditions. These results indicate that the pseudo-second-order kinetic model is more suitable for describing the kinetic adsorption of PS[C_4mim][C272] for V(V), and the adsorption process is mainly chemical reaction.

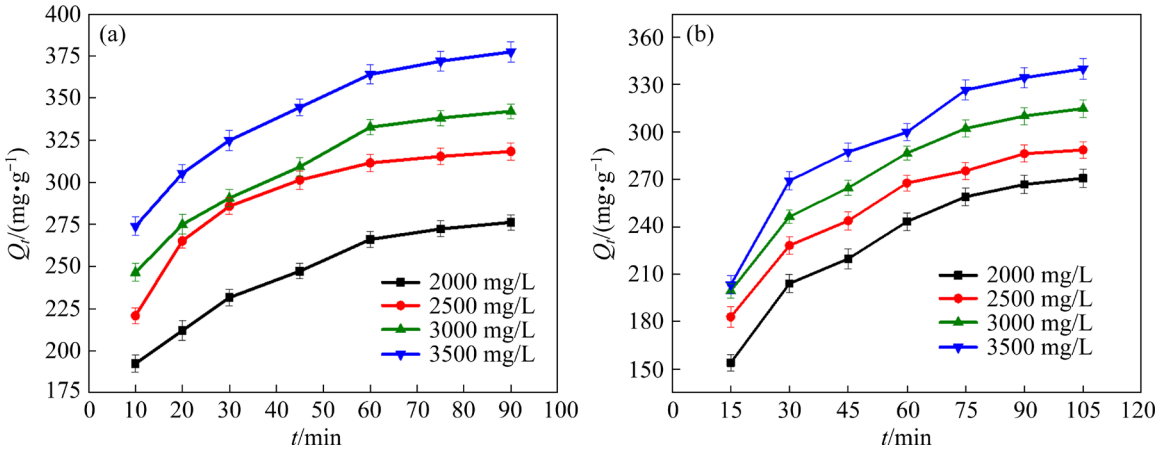

Fig. 3 Effects of vanadium concentrations on adsorption properties of PS[C_4mim][C272] under ultrasound (200 W) (a) and conventional oscillation (b)

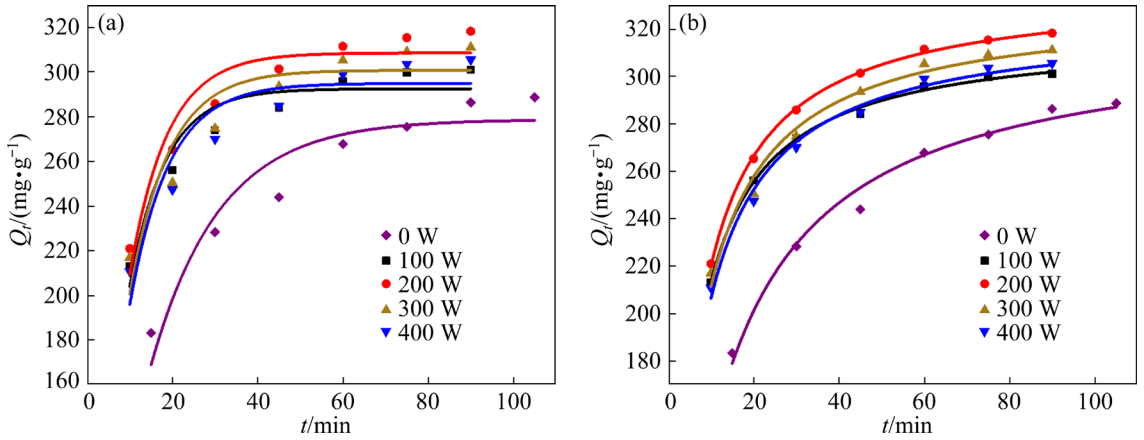

Fig. 4 Fitting curves of pseudo-first-order (a) and pseudo-second-order (b) kinetic models for adsorption process of PS[C_4mim][C272]

Table 1 Fitting parameters of pseudo-first-order and pseudo-second-order kinetic models under different ultrasonic powers

Ultrasonic power/W	Pseudo-first-order model			Pseudo-second-order model		
	k_1/min^{-1}	Q_e/(mg·g^{-1})	R^2	k_2/(g·mg^{-1}·min^{-1})	Q_e/(mg·g^{-1})	R^2
0	0.0621	278.8	0.9113	0.00027	320.2	0.9859
100	0.1196	292.6	0.9211	0.00044	318.5	0.9978
200	0.1135	308.6	0.9192	0.00050	337.7	0.9993
300	0.1098	300.9	0.8660	0.00054	330.4	0.9852
400	0.1091	295.0	0.8795	0.00056	324.3	0.9904

From Table 1, it can be seen that the adsorption rate constant of the pseudo-second-order model increases with the increase in ultrasonic power from 0 to 400 W. The increase of Q_e can be attributed to the ultrasonic cavitation effect that enhances the internal diffusion of the solute [41]. The ultrasonic waves push the vanadium oxyanions into the deep pores of PS[C_4mim][C272], increasing the active interface of PS[C_4mim][C272] and generating additional active adsorption sites [42].

3.4 Control mechanism of adsorption process

3.4.1 Shrinking core model analysis

The non-homogeneous SCM was used to fit the data in Fig. 2 and evaluate the kinetic mechanism of the adsorption process. The rate-controlling step of the adsorption process was preliminarily determined to be either liquid film diffusion, intra-particle diffusion, or chemical reaction. Three fitting curves are shown in Figs. 5(a−c). The R^2 of SCM is presented in Table 2. The results show that the intra-particle diffusion step fit well the adsorption process of PS[C_4mim][C272], and the curve approaches a straight line. Additionally, the R^2 of intra-particle diffusion is the highest among the three mechanisms, especially at an ultrasonic power of 200 W. This indicates that intra-particle diffusion might be the rate-controlling step of the adsorption process. However, the linear deviation of the three kinetic models fitted is slightly more apparent as the ultrasonic power increased.

3.4.2 Weber−Morris internal diffusion model fitting

The Weber−Morris model represents an internal diffusion model commonly used to analyze the controlling step in a reaction and determine the intra-particle diffusion rate constant of the adsorbent. The effect of adsorption time on the adsorption performance of PS[C_4mim][C272] was investigated, and the experimental data were fitted to Eq. (10) to verify whether intra-particle diffusion was the rate-controlling step of the adsorption process. The fitting curve is shown in Fig. 5(d). The internal diffusion rate constant and the R^2 are presented in Table 3.

As shown in Table 3, the R^2 is the smallest under conventional oscillation, which is 0.9460. Under ultrasound, the R^2 ranges from 0.95 to 0.98.

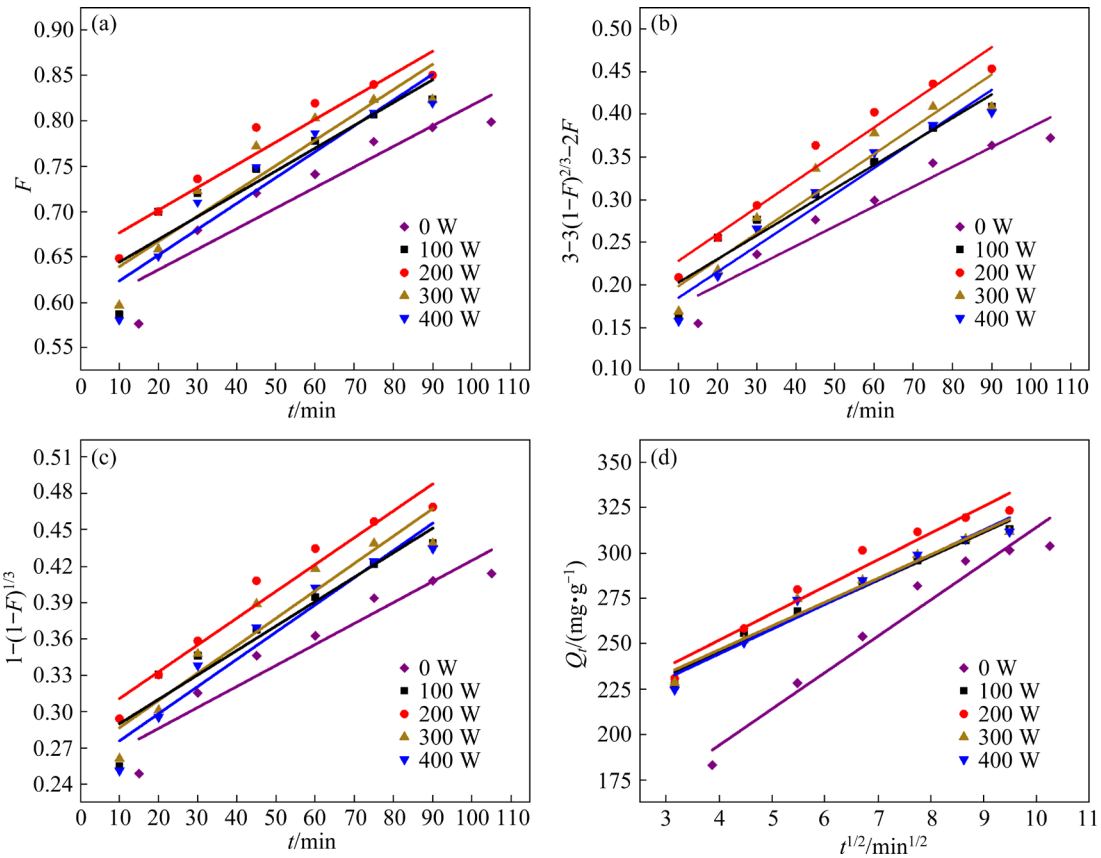

Fig. 5 Fitting curves of liquid film diffusion control mechanism (a), intra-particle diffusion control mechanism (b), chemical reaction control mechanism (c), and Weber−Morris intra-particle diffusion model (d)

Table 2 Goodness of fit of SCM

Ultrasonic power/W	R^2		
	$F-t$	$[3-3(1-F)^{2/3}-2F]-t$	$[1-(1-F)^{1/3}]-t$
0	0.8678	0.9309	0.9122
100	0.8517	0.9311	0.9096
200	0.9230	0.9615	0.9542
300	0.8711	0.9208	0.9083
400	0.8961	0.9512	0.9366

Table 3 Fitting parameters of Weber−Morris model

Ultrasonic power/W	k_{id}/(mg·g^{-1}·min$^{-1/2}$)	R^2
0	20.00	0.9460
100	13.16	0.9789
200	14.53	0.9558
300	12.94	0.9650
400	13.47	0.9598

The internal diffusion rate constant of PS[C$_4$mim][C272] is the largest when the ultrasonic power is 200 W, while the R^2 is the smallest. Therefore, it can be inferred that under the ultrasonic power of 200 W, ultrasound reduced the thickness of the boundary layer around the adsorbent particles, thus reducing the resistance of the liquid film diffusion mechanism [43]. This further enhances the internal diffusion process of the solute and weakens the controlling effect of the intra-particle diffusion mechanism. The combination of ultrasound radiation and mechanical stirring provided the maximum possible for the adsorbent to adsorb V(V) from the solution. This phenomenon can be explained by strong convective transport within the reaction system [44].

3.5 Influence of ultrasonic field on intra-particle diffusion coefficient

Based on the above analysis, it can be inferred that the effect of ultrasound mainly affects the adsorption process of PS[C$_4$mim][C272] by changing the diffusion coefficient of the internal diffusion step of the particles. Therefore, the pseudo-first-order model, SCM, and double driving force model were used to calculate the internal diffusion coefficient under different ultrasonic powers.

3.5.1 Pseudo-steady model

Under the appropriate ultrasonic power, the internal diffusion step of the particles is the rate-controlling step of the adsorption process. The pseudo-steady-state adsorption rate model was used to analyze the kinetic data and calculate the internal diffusion coefficient of the adsorption process. The pseudo-steady-state kinetic equation is shown in Eq. (15):

$$\frac{\mathrm{d}Q}{\mathrm{d}t}=k(C_0-C_e) \tag{15}$$

where k is the diffusion coefficient of the adsorption process (L·g^{-1}·min)).

It can be seen from Eqs. (4) and (15) that the diffusion coefficient (k_1) of the pseudo-first-order kinetic model is proportional to the adsorption rate constant (k). Therefore, assuming the diffusion coefficient of the adsorption process under conventional oscillation conditions is k_0, the diffusion coefficient under different ultrasonic powers can be calculated using Eq. (15), as shown in Table 4. When the ultrasonic power reaches 200 W, the diffusion coefficient is 1.828 times the value of k_0.

Table 4 Diffusion coefficients for adsorption process by pseudo-first-order model under different ultrasonic powers

Ultrasonic power/W	k_1/min^{-1}	k/(L·g^{-1}·min)
0	0.0621	k_0
100	0.1196	1.926k_0
200	0.1135	1.828k_0
300	0.1098	1.768k_0
400	0.1091	1.757k_0

3.5.2 Shrinking core model

According to the SCM fitting results, the internal diffusion coefficients of the adsorption process can be calculated by Eqs. (6)−(8). Assuming the internal diffusion coefficient of the adsorption process under conventional oscillation is $\bar{D}_0$, the internal diffusion coefficient at different ultrasonic powers can be calculated, as shown in Table 5. The results indicate that the internal diffusion coefficient of vanadium on PS[C$_4$mim][C272] increases initially and then decreases with increasing ultrasonic power. When the ultrasonic power is 200 W, the internal diffusion coefficient is 1.348 times the value of $\bar{D}_0$.

3.5.3 Double-driving force model

The double-driving force model is one of the adsorption kinetics models that can be used to

Table 5 Diffusion coefficients for adsorption process by SCM under different ultrasonic powers

Ultrasonic power/W	$\frac{6\bar{D}C_0}{\alpha C_{so}r^2}$/(g·s^{-1}·L^{-1})	$\bar{D}$/(m^2·s^{-1})
0	0.0023	$\bar{D}_0$
100	0.0028	1.217$\bar{D}_0$
200	0.0031	1.348$\bar{D}_0$
300	0.0031	1.348$\bar{D}_0$
400	0.0030	1.304$\bar{D}_0$

calculate the diffusion coefficient of the adsorption process. Therefore, the calculated internal diffusion coefficients (D) and the R^2 based on Eq. (11), are shown in Table 6. From Fig. 6, it can be observed that there is a good linear relationship in the adsorption data under different ultrasonic powers. With the increase of ultrasonic power, the slope of the fitting line decreases first and then increases. Assuming that the internal diffusion coefficient of the adsorption process under conventional oscillation is D_0, the internal diffusion coefficient

Table 6 Calculation of diffusion coefficient for adsorption process by double-driving force model under different ultrasonic powers

Ultrasonic power/W	R^2	$\frac{D\pi^2}{r^2}$/s^{-1}	D/(m^2·s^{-1})
0	0.9813	0.0180	D_0
100	0.9330	0.0189	1.050D_0
200	0.9667	0.0218	1.211D_0
300	0.9241	0.0213	1.183D_0
400	0.9625	0.0209	1.161D_0

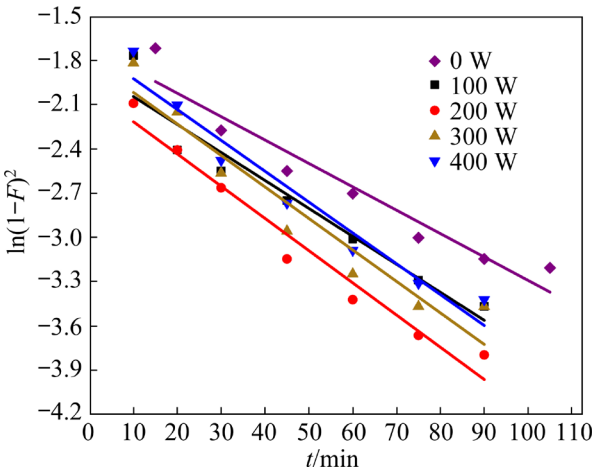

Fig. 6 Fitting curve of double-driving force model

under different ultrasonic powers can be obtained by calculating the slope of each line in Fig. 6. When the ultrasonic power reaches 200 W, the internal diffusion coefficient is 1.211 times the value of D_0 under conventional oscillation.

The fitting results above show the analyses from the pseudo-first-order model, SCM, and double-drive force model are basically consistent. When the ultrasonic power is 200 W, the internal diffusion coefficient of the adsorption process of PS[C_4mim][C272] is 1.2−1.9 times that of conventional oscillation. The increase in diffusion coefficient of PS[C_4mim][C272] during adsorption process under ultrasound can be explained by the cavitation effect of ultrasound.

3.6 Influence of ultrasound on adsorption isotherm

The equilibrium relationship between vanadium in solution and PS[C_4mim][C272] was studied at room temperature, and adsorption performances were investigated at different ultrasonic powers and vanadium concentrations. In order to better quantify the adsorption data and reveal the interaction between V(V) and active adsorption sites in PS[C_4mim][C272], the Langmuir and Freundlich models were used to nonlinearly fit the experimental data to determine the isothermal adsorption equilibrium relationship, as shown in Figs. 7(a) and (b), respectively. The fitting parameters of the corresponding models are listed in Table 7.

Table 7 shows that the Langmuir isotherm model exhibits significantly higher R^2 values (0.9758−0.9967) compared to the Freundlich isotherm model (0.9339−0.9855), indicating a better fit to the experimental data. This suggests that the Langmuir isotherm model describes the adsorption process more consistently, as V(V) is adsorbed onto PS[C_4mim][C272] in a monolayer form. The constants of the Langmuir model reached a maximum at an ultrasonic power of 200 W, indicating an improvement in the adsorption performance of PS[C_4mim][C272]. Ultrasonic radiation not only enhances the internal diffusion of vanadium in PS[C_4mim][C272], but also increases the active interface of the internal pores of PS[C_4mim][C272] through interface effects, effectively utilizing the active groups in the deeper pores. However, at ultrasonic powers of 300 and 400 W, more powerful high-pressure shock waves

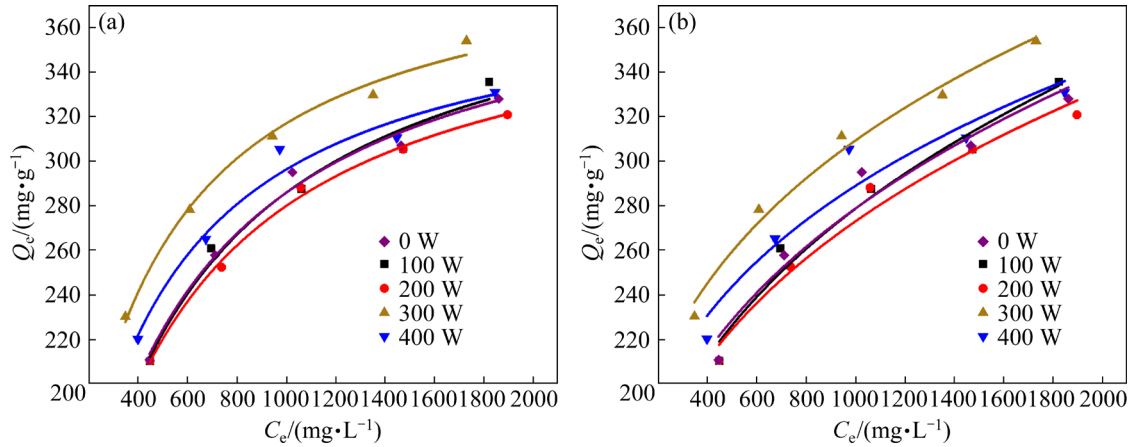

Fig. 7 Fitting curves of Langmuir (a) and Freundlich (b) models under different ultrasonic powers

Table 7 Fitting parameters of Langmuir and Freundlich models under different ultrasonic powers

Ultrasonic power/W	Langmuir isotherm model				Freundlich isotherm model		
	Q_0/(mg·g^{-1})	K_L/ (L·mg^{-1})	R_L	R^2	n/(L·g^{-1})	K_F /(mg·g^{-1}·L$^{1/n}$·mg$^{-1/n}$)	R^2
0	399.1	0.0025	0.5006	0.9778	3.3148	34.67	0.9695
100	384.3	0.0027	0.4908	0.9967	3.5265	38.49	0.9736
200	401.1	0.0038	0.3962	0.9913	4.0534	53.27	0.9855
300	381.4	0.0035	0.4283	0.9758	3.9271	52.56	0.9339
400	393.6	0.0027	0.4848	0.9885	3.4833	38.36	0.9553

and acoustic eddy currents can cause some V(V) and IL to desorb from the surface of PS[C$_4$mim][C272] pores, reducing the adsorption performance of PS[C$_4$mim][C272]. The separation factor (R_L) values of PS[C$_4$mim][C272] range from 0.3962 to 0.5006, falling within the favorable adsorption range of 0−1. This indicates that under the experimental conditions, the adsorption process of PS[C$_4$mim][C272] for V(V) is relatively easy to occur [45]. The adsorption constant (n) is associated with the adsorption strength of the adsorbate on the adsorbent. A higher n value indicates a stronger adsorption strength [46]. This also confirms that ultrasonic assistance has improved the adsorption process of PS[C$_4$mim][C272] for V(V).

3.7 Influence of ultrasound on recycling of PS[C$_4$mim][C272]

As an ideal metal ion adsorbent, it is crucial to examine its ability to be reused. Therefore, the changes in the adsorption performance of PS[C$_4$mim][C272] during 10 adsorption−desorption cycles were studied under ultrasonic-assisted and conventional oscillation. The recycling of PS[C$_4$mim][C272] was evaluated, and the influences of ultrasound on the adsorption performance and cyclic stability of PS[C$_4$mim][C272] were analyzed. The adsorption time is their equilibrium time in Section 3.1. After adsorption, PS[C$_4$mim][C272] was desorbed using a 4 mol/L $NH_3·H_2O$ solution [34], and the desorption rate was greater than 99% each time. The equilibrium adsorption capacity of PS[C$_4$mim][C272] in each cycle under ultrasonic-assisted and conventional oscillation are shown in Figs. 8(a) and (b), respectively.

As can be seen in Fig. 8, the adsorption capacity of PS[C$_4$mim][C272] did not significantly change during the adsorption−desorption cycle under both ultrasonic-assisted and conventional oscillation. In the 10th cycle, the adsorption capacity of PS[C$_4$mim][C272] under ultrasound was 288.59 mg/g, which was 92.62% of the initial value. While under conventional oscillation, the adsorption capacity of PS[C$_4$mim][C272] was 274.93 mg/g, which was 96.30% of the initial value. This is because in the cycling experiment, the

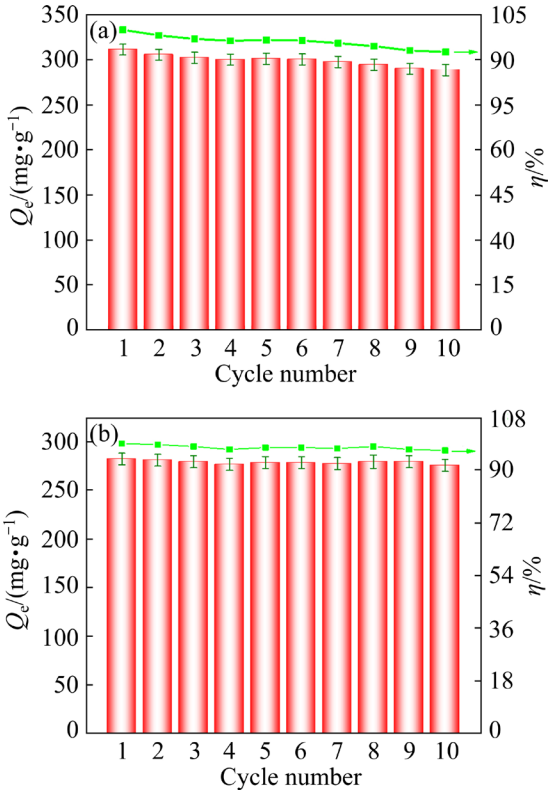

Fig. 8 Reusability of PS[C_4mim][C272] under ultrasonic-assisted (200 W) (a) and conventional oscillation (b)

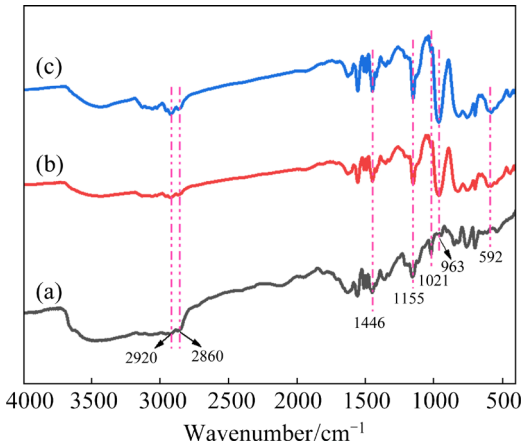

Fig. 9 FTIR spectra of PS[C_4mim][C272] before adsorption (a), after ultrasonic-assisted adsorption (b), and after conventional oscillation adsorption (c)

cavitation effect of ultrasound generates microjet shock waves that erode and peel off the loaded IL, leading to a more significant decrease in the adsorption capacity of PS[C_4mim][C272] under ultrasonic-assisted compared to conventional oscillation. The above results indicate that PS[C_4mim][C272] exhibits good cycle stability, and ultrasound has little effect on its adsorption performance and reusability. Combined with the results of adsorption kinetics, PS[C_4mim][C272] can be considered as a potential adsorbent for the removal or recovery of vanadium.

The FTIR spectroscopy analysis was used to characterize the functional groups of PS[C_4mim][C272] before and after adsorption. As shown in Fig. 9, PS[C_4mim][C272] contains imidazole rings, and the absorption peak at 1446 cm^{-1} is characteristic of the imidazole ring skeleton vibration. The absorption peaks at 2920 and 2860 cm^{-1} are caused by the asymmetric stretching vibration of C—H_2 and the symmetric stretching vibration of C—H_3 on the imidazole ring, respectively [47]. In Fig. 9(a), the characteristic absorption peaks at 1155 and 1021 cm^{-1} are attributed to the stretching vibrations of P—O and P═O in [C272]$^-$, respectively. In Figs. 9(b) and (c), the disappearance of the characteristic peak of P═O indicates that P═O is disrupted and oxygen atoms is coordinate with the central V(V) [40]. The absorption peaks at 963 and 592 cm^{-1} are related to the stretching vibrations of V═O and V—O [40]. It can be observed that there are no significant differences in the FTIR spectra of PS[C_4mim][C272] after adsorption under ultrasonic-assisted and conventional oscillation conditions, indicating that the main structure of PS[C_4mim][C272] is not affected by ultrasound.

Figure 10 shows the SEM images of the microstructure of PS[C_4mim][C272] before and after adsorption under ultrasonic-assisted and conventional oscillation. The low-magnification scanning electron microscope images (enlarged 200−300 times) show that PS[C_4mim][C272] is spherical. A layer of vanadium element is observed to cover the surface of the adsorbed PS[C_4mim][C272] from the scanning electron microscope images at 2500 times magnification. It can be seen from Fig. 10 that the integrity of PS[C_4mim][C272] is well-maintained. This further proves that the ultrasonic waves and mechanical oscillation do not damage the overall structure of PS[C_4mim][C272] during the adsorption process.

3.8 Adsorption performance

The partial study of adsorption vanadium was analyzed to evaluate the effectiveness of introducing ultrasonic-assisted to improve the adsorption performance in this study. The experimental results of this study were compared

with those of other studies based on the reaction method, adsorption equilibrium time, and maximum adsorption capacity, as shown in Table 8.

As can be seen from Table 8, the maximum adsorption capacities of ion exchange resins Lewatit MP800, Lewatit MP62WS, Lewatit TP260,

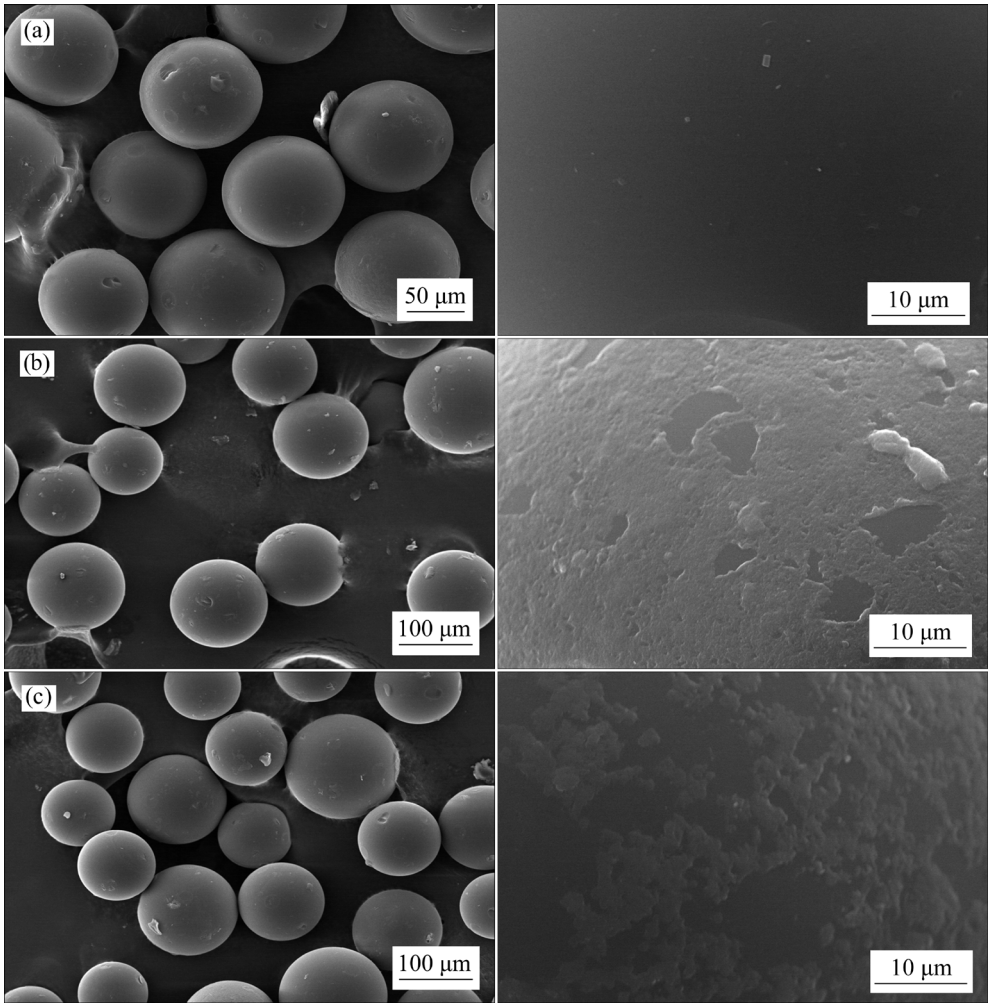

Fig. 10 SEM images of PS[C_4mim][C272] before adsorption (a), after ultrasonic-assisted adsorption (b), and after conventional oscillation adsorption (c)

Table 8 Comparison of adsorption performance of PS[C_4mim][C272] and other adsorbents toward vanadium on basis of reaction method, adsorption equilibrium time, and maximum adsorption capacity

Adsorbent	Processed object	Treatment method	Adsorption equilibrium time/min	Maximum adsorption capacity/(mg·g^{-1})	Source
Lewatit MP800	V(V)	Conventional oscillation	1440	9.70	[48]
Lewatit MP62WS	V(V)	Conventional oscillation	1440	6.65	[48]
Lewatit TP260	V(V)	Conventional oscillation	1440	3.75	[48]
Lewatit® MonoPlus TP 209 XL	V(V)	Conventional oscillation	120	32.86	[49]
Lewatit® MonoPlus TP 207	V(V)	Conventional oscillation	120	31.66	[49]
Dowex™ M4195	V(V)	Conventional oscillation	120	38.65	[49]
PS[C_4mim][C272]	V(V)	Conventional oscillation	90	285.49	This study
PS[C_4mim][C272]	V(V)	Ultrasonic-assisted	60	311.58	This study

Lewatit® MonoPlus TP 209 XL, Lewatit® MonoPlus TP 207, Dowex™ M4195 for vanadium were 9.70, 6.65, 3.75, 32.86, 31.66 and 38.65 mg/g, respectively. Research has found that PS[C_4mim][C272] has a higher adsorption capacity for vanadium at 285.49 mg/g compared to other adsorbents. Furthermore, the adsorption process of PS[C_4mim][C272] for vanadium can reach equilibrium faster (within only 60 min) under ultrasonic-assisted conditions compared to other studies (120−1440 min). This is because ultrasound is able to widen the pores in the internal structure of PS[C_4mim][C272], reducing pore blockage and promoting solute transport, which significantly increases the adsorption capacity and short the adsorption time [50]. This indicates that the introduction of ultrasonic wave is a feasible method to improve the adsorption properties of adsorbents.

4 Conclusions

(1) The equilibrium adsorption capacity of PS[C_4mim][C272] for V(V) reached a maximum value of 311.58 mg/g at an ultrasonic power of 200 W, and the adsorption capacity increased with increasing vanadium concentration.

(2) Kinetic studies showed that the adsorption process of PS[C_4mim][C272] for vanadium followed the pseudo-second-order kinetic model, and the adsorption rate constantly increased with increasing ultrasonic power. The fitting results of SCM and Weber−Morris intra-particle diffusion models showed that the rate-controlling mechanism of adsorption process was mainly intra-particle diffusion. At an ultrasonic power of 200 W, the internal diffusion coefficient reached a value of 1.2−1.9 times that under conventional oscillation.

(3) The fitted adsorption isothermal model showed that the adsorption process of PS[C_4mim][C272] for V(V) was in accordance with the Langmuir isothermal model, and V(V) was adsorbed onto PS[C_4mim][C272] in the form of a monolayer. The cyclic test results showed that PS[C_4mim][C272] had good reusability under ultrasound, and the adsorption capacity remains at 92.62% of the initial value after the tenth cycle.

(4) FTIR and SEM analysis showed that ultrasonic radiation and conventional oscillation did not damage the overall structure and molecular structure of PS[C_4mim][C272] during the adsorption process. Therefore, ultrasonic-assisted adsorption process has essential significance for the enrichment of vanadium in acidic leachate.

CRediT authorship contribution statement

Jia-hao ZHOU: Conceptualization, Methodology, Investigation, Data curation, Formal analysis, Software, Writing − Original draft; **Shen-xu BAO:** Resources, Funding acquisition, Project administration, Supervision, Writing − Review & editing; **Yi-min ZHANG:** Supervision, Project administration, Validation; **Bo CHEN:** Formal analysis, Conceptualization, Methodology; **Yu LIANG:** Conceptualization, Software; **Xiao-chuan HOU** and **Si-yuan YANG:** Supervision; **Yang PING:** Methodology.

Declaration of competing interest

The authors declare that they have no known competing financial interests or personal relationships that could have appeared to influence the work reported in this paper.

Acknowledgments

This research was financially supported by the National Natural Science Foundation of China (No. 52074204), and Key R&D Program of Zhejiang Province, China (No. 2022C03061).

References

[1] LIU Yin, LIU Zheng, MNICHOWICZ B, HARINATH A V, LI Hui-ling, BAHRAMI B. Chemical deactivation of commercial vanadium SCR catalysts in diesel emission control application [J]. Chemical Engineering Journal, 2016, 287: 680−690.

[2] CHEN Bo, BAO Shen-xu, ZHANG Yi-min. Effects of key impurities (Al, Fe, P, Si and Na) on the precipitation process of vanadium in the novel ultrasound-assisted precipitation system [J]. Hydrometallurgy, 2024, 224: 106233.

[3] DENG Zhi-gan, WEI Chang, FAN Gang, LI Min-ting, LI Cun-xiong, LI Xing-bin. Extracting vanadium from stone-coal by oxygen pressure acid leaching and solvent extraction [J]. Transactions of Nonferrous Metals Society of China, 2010, 20(S): 118−122.

[4] COCHECI L, LUPA L, TOLEA N S, MUNTEAN C, NEGREA P. Sequential use of ionic liquid functionalized Zn−Al layered double hydroxide as adsorbent and photocatalyst [J]. Separation and Purification Technology, 2020, 250: 117104.

[5] DONG Zhen, ZHAO Long. Covalently bonded ionic liquid onto cellulose for fast adsorption and efficient separation of Cr(VI): Batch, column and mechanism investigation [J]. Carbohydrate Polymers, 2018, 189: 190−197.

[6] ZHOU Jia-hao, BAO Shen-xu, ZHANG Yi-min, CHEN Bo, LIANG Yu, HOU Xiao-chuan, YANG Si-yuan, PING Yang,

ZHOU Zi-chen. Adsorption property and mechanism of vanadium(V) by supported bifunctionalized ionic liquid [J]. Colloids and Surfaces A: Physicochemical and Engineering Aspects, 2024, 681: 132753.

[7] CHEN Bo, BAO Shen-xu, ZHANG Yi-min, LI Chao. Reactive crystallization of ammonium polyvanadate from vanadium-bearing solution assisted by efficient ultrasound irradiation: Crystallization characteristics and growth process [J]. Journal of Materials Research and Technology, 2023, 25: 667−680.

[8] DOU Jin-xiao, YU Jiang-long, TAHMASEBI A, YIN Feng-kui, GUPTA S, LI Xian-chun, LUCAS J, NA Chuan, WALL T. Ultrasonic-assisted preparation of highly reactive Fe−Zn sorbents supported on activated-char for desulfurization of COG [J]. Fuel Processing Technology, 2015, 135: 187−194.

[9] LI Zhong, LI Xiang-bin, XI Hong-xia, HUA Ben. Effects of ultrasound on adsorption equilibrium of phenol on polymeric adsorption resin [J]. Chemical Engineering Journal, 2002, 86(3): 375−379.

[10] JI Jian-bing, LU Xiang-hong, XU Zhi-chao. Effect of ultrasound on adsorption of Geniposide on polymeric resin [J]. Ultrasonics Sonochemistry, 2006, 13(5): 463−470.

[11] BREITBACH M, BATHEN D. Influence of ultrasound on adsorption processes [J]. Ultrasonics Sonochemistry, 2001, 8(3): 277−283.

[12] ZHANG Ying, LI Shu-fen, WU Xi-wen, ZHAO Xing. Macroporous resin adsorption for purification of flavonoids in houttuynia cordata thunb [J]. Chinese Journal of Chemical Engineering, 2007, 15(6): 872−876.

[13] DING Wei, BAO Shen-xu, ZHANG Yi-min, REN Liu-yi, XIN Chun-fu., CHEN Bo, LIU Bo, XIAO Jun-hui, HOU Xiao-chuan. Stepwise recycling of valuable metals from spent lithium-ion batteries based on in-situ thermal reduction and ultrasonic-assisted water leaching [J]. Green Chemistry, 2023, 25: 6652−6665.

[14] BREITBACH M, BATHEN D, SCHMIDT-TRAUB H. Desorption of a fixed-bed adsorber by ultrasound [J]. Ultrasonics, 2002, 40(1−8): 679−682.

[15] AHMAD M, WANG Ji-qi, YANG Zuo-ting, ZHANG Qiu-yu, ZHANG Bao-liang. Ultrasonic-assisted preparation of amidoxime functionalized silica framework via oil-water emulsion method for selective uranium adsorption [J]. Chemical Engineering Journal, 2020, 389: 124441.

[16] JING Guo-hua, ZHOU Zuo-ming, SONG Lei, DONG Mei-xia. Ultrasound enhanced adsorption and desorption of chromium (VI) on activated carbon and polymeric resin [J]. Desalination, 2011, 279(1/2/3): 423−427.

[17] YAO Ye, YANG Kun, LIU Shi-qing. Study on the performance of silica gel dehumidification system with ultrasonic-assisted regeneration [J]. Energy, 2014, 66: 799−809.

[18] LEE D, JANG Y H, KANNATEY-ASIBU E. Numerical analysis of pseudostatic frictional contact of an elastic block under combined normal and tangential cyclic loading [J]. International Journal of Mechanical Sciences, 2012, 64(1): 174−183.

[19] ZHENG Tao, DU Jun, YUAN Yi, WU Shuo, JIN Ying-lan, SHI Qing-lei, WANG Xiao-han, LIU Lan-xiang. Effect of low intensity transcranial ultrasound (LITUS) on post-traumatic brain edema in rats: evaluation by isotropic 3-dimensional T2 and multi-TE T2 weighted MRI [J]. Frontiers in Neurology, 2020, 11: 578638.

[20] WANG Long, SUN Yuan, WANG Shi-yang, ZHANG Ting-an, LU Guo-zhi. Leaching mechanism of strategic metals from superalloy scrap under ultrasonic cavitation [J]. Transactions of Nonferrous Metals Society of China, 2023, 33(1): 304−314.

[21] DING Wei, BAO Shen-xu, ZHANG Yi-min, XIN Chun-fu., CHEN Bo, LI Jia, LIU Bo, XIA Yi-feng, HOU Xiao-chuan, XU Kai-hua. Sustainable regeneration of high-performance cathode materials from spent lithium-ion batteries through magnetic separation and coprecipitation [J]. Journal of Cleaner Production, 2024, 438: 140798.

[22] ELWAKEEL K Z, SHAHAT A, AL-BOGAMI A S, WIJESIRI B, GOONETILLEKE A. The synergistic effect of ultrasound power and magnetite incorporation on the sorption/ desorption behavior of Cr(VI) and As(V) oxoanions in an aqueous system [J]. Journal of Colloid and Interface Science, 2020, 569: 76−88.

[23] ENTEZARI M H, GHOWS N, CHAMSAZ M. Ultrasound facilitates and improves removal of Cd(II) from aqueous solution by the discarded tire rubber [J]. Journal of Hazardous Materials, 2006, 131(1/2/3): 84−89.

[24] WEN Zhen-qian, HUANG Kai-hua, NIU Yu-qing, YAO Yi-xuan, WANG Shuai, CAO Zhan-fang, ZHONG Hong. Kinetic study of ultrasonic-assisted uranium adsorption by anion exchange resin [J]. Colloids and Surfaces A: Physicochemical and Engineering Aspects, 2020, 585: 124021.

[25] ZHUMAN B, KHALIFEH H A, ZUBURTIKUDIS I, KUMAR M, ARAFAT H A, NASHEF E. Ionic liquid functionalized graphene oxide for the adsorption of Ca^{2+} and Mg^{2+} ions from saline aqueous feed [J]. Korean Journal of Chemical Engineering, 2023, 40(5): 1176−1185.

[26] ZHENG Ru-wei, BAO Shen-xu, ZHANG Yi-min, CHEN Bo. Synthesis of di-(2-ethylhexyl) phosphoric acid (C272A)-tributyl phosphate (TBP) impregnated resin and application in adsorption of vanadium(IV) [J]. Minerals, 2018, 8(5): 206.

[27] BAO Shen-xu, CHEN Bo, ZHANG Yi-min, REN Liu-yi, XIN Chun-fu, DING Wei, YANG Si-yuan, ZHANG Wen-cai. A comprehensive review on the ultrasound-enhanced leaching recovery of valuable metals: Applications, mechanisms and prospects [J]. Ultrasonics Sonochemistry. 2023, 98: 106525.

[28] YU Chen, BAO Shen-xu, ZHANG Yi-min, CHEN Bo. Separation and adsorption of V(V) from canadium-containing solution by TOMAC-impregnated resins [J]. Chemical Engineering Research and Design, 2021, 174: 405−413.

[29] VINCO J H, BOTELHO A B Jr, DUARTE H A, ESPINOSA D C R, TENÓRIO J A S. Kinetic modeling of adsorption of vanadium and iron from acid solution through ion exchange resins [J]. Transactions of Nonferrous Metals Society of China, 2022, 32(7): 2438−2450.

[30] WEBER W Jr, MORRIS J C. Kinetics of adsorption on carbon from solution [J]. Journal of the Sanitary Engineering

Division, American Society of Civil Engineers, 1963, 89(2): 31−59.

[31] BOYD G E, ADAMSON A W, MYERS L S Jr. The exchange adsorption of ions from aqueous solutions by organic zeolites: Kinetics [J]. Journal of the American Chemical Society, 1947, 69(11): 2836−2848.

[32] CHEN Bo, BAO Shen-xu, ZHANG Yi-min. Synergetic strengthening mechanism of ultrasound combined with calcium fluoride towards vanadium extraction from low-grade vanadium-bearing shale [J]. International Journal of Mining Science and Technology, 2021, 31: 1095−1106.

[33] HUI K S, CHAO C Y H, KOT S C. Removal of mixed heavy metal ions in wastewater by zeolite 4A and residual products from recycled coal fly ash [J]. Journal of Hazardous Materials, 2005, 127(1/2/3): 89−101.

[34] JING Xiao-hua, SUN Zhu-mei, ZHAO Dan-dan, XIA Ling-ling, YE Zi-qing. Efficient separation and recovery of V(V) from Cr (VI) in aqueous solution using new task-specific ionic liquid of $[C_{12}H_{25}NH_3]$[Cyanex272] [J]. Arabian Journal of Chemistry, 2022, 15(10): 104173.

[35] LEÃO V A, LUKEY G C, van DEVENTER J S J, CIMINELLI V S T. The dependence of sorbed copper and nickel cyanide speciation on ion exchange resin type [J]. Hydrometallurgy, 2001, 61(2): 105−119.

[36] KARIMI R, YOUSEFI F, GHAEDI M, DASHTIAN K. Back propagation artificial neural network and central composite design modeling of operational parameter impact for sunset yellow and azur (II) adsorption onto MWCNT and MWCNT-Pd-NPs: Isotherm and kinetic study [J]. Chemometrics and Intelligent Laboratory Systems, 2016, 159: 127−137.

[37] XIE Feng, CHEN Jun-nan, ZHANG Xiao-zhen, XU Bin, WANG Wei. Adsorption mechanism of copper and gold thiosulfates onto activated carbon [J]. Transactions of Nonferrous Metals Society of China, 2023, 33(10): 3210−3221.

[38] KALIDHASAN S, KUMAR A S K, RAJESH V, RAJESH N. An efficient ultrasound assisted approach for the impregnation of room temperature ionic liquid onto Dowex 1 × 8 resin matrix and its application toward the enhanced adsorption of chromium (VI) [J]. Journal of Hazardous Materials, 2012, 213: 249−257.

[39] HAMDAOUI O, NAFFRECHOUX E. An investigation of the mechanisms of ultrasonically enhanced desorption [J]. AIChE Journal, 2007, 53(2): 363−373.

[40] ZHOU Jia-hao, BAO Shen-xu, ZHANG Yi-min, CHEN Bo, LIANG Yu, DING wei, HOU Xiao-chuan, YANG Si-yuan, PING Yang. Adsorption behavior of vanadium(V) by supported imidazolium-based difunctionalized ionic liquid [J]. Journal of Molecular Liquids, 2023, 391: 123245.

[41] OMIDI M H, AZAD F N, GHAEDI M, ASFARAM A, AZQHANDI M H A, TAYEBI L. Synthesis and characterization of Au-NPs supported on carbon nanotubes: Application for the ultrasound assisted removal of radioactive UO_2^{2+} ions following complexation with arsenazo III: Spectrophotometric detection, optimization, isotherm and kinetic study [J]. Journal of Colloid and Interface Science, 2017, 504: 68−77.

[42] HAMDAOUI D. Removal of cadmium from aqueous medium under ultrasound assistance using olive leaves as sorbent [J]. Chemical Engineering and Processing: Process Intensification, 2009, 48(6): 1157−1166.

[43] MARY EALIAS A, SARAVANAKUMAR M P. A critical review on ultrasonic-assisted dye adsorption: Mass transfer, half-life and half-capacity concentration approach with future industrial perspectives [J]. Critical Reviews in Environmental Science and Technology, 2019, 49(21): 1959−2015.

[44] HAMDAOUI O, NAFFRECHOUX E, SUPTIL J, FACHINGER C. Ultrasonic desorption of p-chlorophenol from granular activated carbon [J]. Chemical Engineering Journal, 2005, 106(2): 153−161.

[45] WU Ye-hui-zi, ZHOU Kang-gen, CHEN Wei, LEI Qing-yuan, ZHANG Er-jun, CHENG Yu-yao, JIANG Yang, PENG Chang-hong, JIANG Jun, ZHANG Xue-kai. Chromatographic separation and recovery of Zn(II) and Cu(II) from high-chlorine raffinate of germanium chlorination distillation [J]. Transactions of Nonferrous Metals Society of China, 2022, 32(4): 1336−1350.

[46] IVANENKO V I, MASLOVA M V, EVSTROPOVA P E, GERASIMOVA L G. Purification of saturated $LiNO_3$ solution using titanium phosphate ion-exchanger: Equilibrium study [J]. Transactions of Nonferrous Metals Society of China, 2023, 33(8): 2543−2558.

[47] BASU P B, DEY T K, GHOSH A, BISWAS S B, KHAN A, ISLAM S M. An efficient one-pot synthesis of industrially valuable primary organic carbamates and N-substituted ureas by a reusable Merrifield anchored iron(II)-anthra catalyst [Fe-II(Anthra-Merf)] using urea as a sustainable carbonylation source [J]. New Journal of Chemistry, 2020, 44(6): 2630−2643.

[48] HONG H J, YOO H, JEON J H, KIM H S, LEE J Y. Differential adsorption of vanadium(V) and tungsten(W) on ion exchange resins: A novel approach for separation and recovery of spent catalyst leachate [J]. Journal of Cleaner Production, 2023, 426: 139157.

[49] VINCO J H, BOTELHO A B Jr, DUARTE H A, ESPINOSA D C R, TENÓRIO J A S. Purification of an iron contaminated vanadium solution through ion exchange resins [J]. Minerals Engineering, 2022, 176: 107337.

[50] ZHANG Hong-wei, XU Hai-yin, ZI Hui, TANG Yu-wei, ZHENG Xi-jie, WANG Ping, HUANG Jing, WU Hong-hui, SONG Pei-pei, WU Lin-xin, LIU Ze-chen, MAO Wen-shao, SONG Xin-yang, JIA Mei-ying. Investigation of the redox behavior of biochar-based bipolar electrochemistry in porous media [J]. Chemical Engineering Journal, 2023, 470: 144384.

负载型双官能团离子液体超声辅助钒(V)吸附的动力学研究

周佳豪[1,2]，包申旭[1,2,3]，张一敏[1,2,3,4]，陈 波[1,2]，梁 钰[1,2]，侯晓川[5]，杨思原[1,2]，平 杨[6]

1. 武汉理工大学 关键非金属矿产资源绿色利用教育部重点实验室，武汉 430070；
2. 武汉理工大学 资源与环境工程学院，武汉 430070；
3. 矿物资源加工与环境湖北省重点实验室，武汉 430070；
4. 武汉科技大学 国家环境保护矿冶资源利用与污染控制重点实验室，武汉 430081；
5. 浙江新时代中能循环科技有限公司，绍兴 312000；
6. 中电建生态环境集团有限公司，深圳 518102

摘 要：探讨聚苯乙烯[1-丁基-3-甲基咪唑][双(2,4,4-三甲基戊基)膦酸盐](PS[C4mim][C272])在超声条件下对酸性浸出液中钒(V)的吸附动力学。研究超声功率和钒(V)浓度对 PS[C4mim][C272]吸附性能的影响。结果表明，与常规振荡相比，超声波辐射大大缩短了 PS[C4mim][C272]的吸附平衡时间，提高了其吸附性能。在超声功率为 200 W 时，PS[C4mim][C272]的平衡吸附容量达到最大值 311.58 mg/g。动力学模型拟合结果表明，PS[C4mim][C272]在超声条件下的吸附过程严格遵循准二级动力学模型。利用收缩核模型和韦伯−莫里斯模型进行分析表明，PS[C4mim][C272]的吸附过程主要受颗粒内扩散机制控制。吸附等温模型研究表明，Langmuir 等温模型能有效地拟合 PS[C4mim][C272]在超声下的吸附过程。

关键词：动力学；超声波；钒；聚苯乙烯[1-丁基-3-甲基咪唑][双(2,4,4-三甲基戊基)膦酸盐]；常规振荡；吸附

(Edited by Xiang-qun LI)